



Effects of precursors for manganese-loaded γ - Al_2O_3 catalysts on plasma-catalytic removal of o-xylene



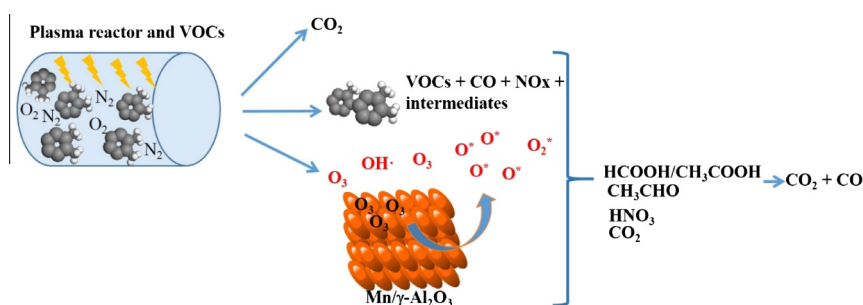
Lian Wang, Hong He^{*}, Changbin Zhang, Yafei Wang, Bo Zhang

State Key Joint Laboratory of Environment Simulation and Pollution Control, Research Center for Eco-Environmental Sciences, Chinese Academy of Sciences, Beijing 100085, China

HIGHLIGHTS

- Effects of precursors and loading amounts on $\text{Mn}/\text{Al}_2\text{O}_3$ catalysts were investigated.
- Catalyst prepared with manganese acetate had the greatest catalytic activity.
- The plasma-catalytic processes greatly decreased the concentrations of O_3 and NO_x .
- More Mn^{4+} and microcrystalline MnO_2 increased catalytic activity.
- Higher proportion of lattice oxygen was responsible for high catalytic activity.

GRAPHICAL ABSTRACT



ARTICLE INFO

Article history:

Received 10 October 2015

Received in revised form 30 November 2015

Accepted 3 December 2015

Available online 12 December 2015

Keywords:

Non-thermal plasma
 $\text{Mn}/\text{Al}_2\text{O}_3$ catalyst
Different precursors
Microcrystalline phase

ABSTRACT

The effects of precursors and Mn loading amounts on $\text{Mn}/\text{Al}_2\text{O}_3$ catalysts for plasma-catalytic removal of o-xylene were systematically investigated. Catalysts were characterized by XRD, XPS, and H_2 -TPR. Experimental results show that o-xylene conversion was greatly increased even at very low specific energy density with addition of $\text{Mn}/\text{Al}_2\text{O}_3$ catalysts. The $\text{Mn}/\text{Al}_2\text{O}_3$ catalyst prepared with a manganese acetate precursor had the highest catalytic activity for o-xylene removal. Among tested loading amounts, 6 wt% Mn loading was the optimum condition for preparation of catalysts for o-xylene conversion. The presence of more Mn^{4+} species, higher proportion of lattice oxygen and microcrystalline MnO_2 phase on the surface of catalysts was responsible for the high catalytic activity for o-xylene removal. To compare with $\text{Mn}/\text{Al}_2\text{O}_3$ catalysts prepared with manganese acetate precursor, α - $\text{MnO}_2/\text{Al}_2\text{O}_3$ with more Mn^{4+} and lattice oxygen on the surface was also prepared. The o-xylene conversion, CO_2 selectivity, and $(\text{CO} + \text{CO}_2)$ (i.e. CO_x) yield increased with introduction of α - $\text{MnO}_2/\text{Al}_2\text{O}_3$ catalyst, which was due to the high oxidation ability of α - $\text{MnO}_2/\text{Al}_2\text{O}_3$ induced by higher amounts of Mn^{4+} and lattice oxygen. The concentrations of O_3 and NO_x byproducts greatly decreased when catalysts were used. The FT-IR spectrum show that CH_3CHO , O_3 , NO_x and HNO_3 products were formed without catalyst, while $\text{HCOOH}/\text{CH}_3\text{COOH}$ formation occurred with catalysts.

© 2015 Elsevier B.V. All rights reserved.

1. Introduction

Benzene, toluene, and xylene (BTX) are the typical volatile organic compounds (VOCs) and harmful to the environment and

human health. Removal of BTX for purification of indoor air and gaseous industrial streams is very important and necessary [1,2]. Recently, non-thermal plasma (NTP) technology is regarded as a promising method since NTP could efficiently remove BTX at ambient conditions through generating strong oxidizing agents like ozone, hydroxyl radical, atomic oxygen, etc [3,4]. However, the main drawback of NTP for BTX removal is inevitable byproducts

^{*} Corresponding author. Tel./fax: +86 10 62849123.

E-mail address: honghe@rcees.ac.cn (H. He).

formation and low CO₂ selectivity because there is not enough energy of radicals for complete oxidation of BTX [4]. To overcome these disadvantages of NTP, the combination of NTP and catalysis has aroused great interest to study the removal of BTX [4–16]. The byproducts formed during the plasma treatment could be oxidized by adding catalyst to abate the production of byproducts and increase CO₂ selectivity.

For plasma-catalytic process to remove BTX, one of the crucial issues is to find an appropriate catalyst with good catalytic performance. In recent years, Mn containing catalysts have been widely explored, which had high catalytic activity for BTX removal in plasma-catalytic process [5,6,8–10]. Manganese oxide (MnO_x) is the most active metal oxide catalyst for decomposition of ozone to generate atomic oxygen species which play an important role for oxidation of VOCs [15–17]. Guo et al. have confirmed that manganese oxide/alumina/NF was the most effective catalyst for toluene removal among copper oxide, iron oxide, cobalt oxide, and manganese oxide loaded catalysts in plasma-catalytic process [8]. Zhu et al. have investigated the combination of NTP and MnO_x/Al₂O₃ catalysts for removal of BTX, and found that MnO_x/Al₂O₃ catalysts could lead to BTX total conversion and reduce the emission of O₃ and NO₂ [9]. MnO_x/SMF catalysts showed higher activity toward VOCs oxidation than CoO_x/SMF catalysts [10]. According to the above reports, MnO_x catalysts are promising to BTX conversion used in plasma-catalytic process. The catalytic activities of some transition metal doped Mn oxides have also been compared [18,19]. As the active species, the structure of Mn in catalyst was important for VOCs removal via combination of NTP and catalysis. Therefore, the effects of Mn valence and preparation conditions on BTX removal via combination of NTP and Mn catalysts need to be systematically investigated.

In this work, Mn/Al₂O₃ catalysts were prepared with different precursors and loading amounts, and α-MnO₂/Al₂O₃ was used for comparison. We also tested their activities for o-xylene removal in a dielectric barrier discharge (DBD) plasma system by introducing the above catalysts after the discharge zone. The conversion of o-xylene, CO₂ selectivity, carbon yield, decomposition products and discharge byproducts were investigated. Catalysts were characterized by XRD, XPS, and H₂-TPR methods. The effects of preparation condition on the chemical properties such as Mn valence, lattice oxygen contents, and redox properties were analyzed and subsequently correlated with their catalytic activities.

2. Experimental

2.1. Experimental setup and methods

A schematic diagram of the experimental setup is shown in Fig. 1, which includes a cylindrical plasma-catalysis reactor with inner high-voltage electrode, an o-xylene generator with reaction gas, and some analytical instruments for products measurements. The discharge-catalysis reactor had a coaxial geometry (inner diameter 8 mm, outer diameter 18 mm, and length 400 mm) with a quartz tube as dielectric between the inner high-voltage electrode (aluminum, diameter 8 mm and length 100 mm) and the grounded electrode (aluminum foil, diameter 18 mm and length 100 mm) on the outer quartz tube wall to form a 100 mm length DBD zone. The gas discharges were produced by a high-frequency AC high-voltage power supply source. In addition, catalysts (1.5 g, 40–60 mesh) were placed after the discharge zone. The gas o-xylene was produced by bubbling with N₂ and mixed with O₂ and N₂ before the reactor to achieve the mixed reactant feed that composed of 9 ppm o-xylene, 20 vol% O₂ and 80 vol% N₂ (total flow rate = 6 L min⁻¹). The AC power was supplied to start the electro-discharge and reaction when the concentration of

o-xylene reached a steady state. All experiments were repeated in triplicate.

Discharge power was measured by the V–Q Lissajous program. The charge Q was measured from the voltage across a capacitor of 100 nF connected in series to the ground electrode. The applied voltage was measured with a 1000:1 high-voltage probe (Tektronix TPP0201). The waveforms of the charge Q and the applied voltage were monitored using a digital oscilloscope (Tektronix TDS 2012c) and plotted to obtain the Lissajous diagram.

The o-xylene conversion, CO₂ selectivity, CO_x yield, and specific energy density in the gas phase were defined as follows:

o-xylene conversion efficiency (%)

$$= [\text{o-xylene}]_{\text{outlet}} / [\text{o-xylene}]_{\text{inlet}} \times 100$$

Carbon dioxide selectivity (%) = [CO₂]/8[C₈H₁₀]_{conversion} × 100

Carbon dioxide and carbon monoxide yield:

$$\text{CO}_x \text{ yield (\%)} = ([\text{CO}] + [\text{CO}_2]) / 8[\text{C}_8\text{H}_{10}]_{\text{conversion}} \times 100$$

Specific energy density: SED (J/L)

$$= \text{discharge power (W)} / \text{gas flow rate (L/min)} \times 60$$

The o-xylene concentration was analyzed online by a GC–MS (Agilent 6890–5973 N, HP 5MS). CO₂ and CO concentrations were analyzed by a GC equipped with FID detector (Shangfen GC-112A, TDX-01 column). O₃ and NO_x concentrations were determined by an O₃ detector (Model 202, 2B Technology) and NO_x detector (Thermal 42i). Other oxidation products were detected by online FT-IR (Thermo Scientific Nicolet is 50).

2.2. Catalyst preparation

Mn/Al₂O₃ catalysts were prepared through an impregnation method by introducing an appropriate amount of γ-Al₂O₃ powder into manganese acetate, manganese chloride, manganese sulfate, or manganese nitrate precursor solutions, and the catalysts were designated as Mn/Al₂O₃-MA, Mn/Al₂O₃-MC, Mn/Al₂O₃-MS, and Mn/Al₂O₃-MN, respectively. The mixed solutions were stirred for 2 h at room temperature, followed by evaporation to dryness in a rotary evaporator at 60 °C. The obtained solids were dried at 100 °C overnight and calcined at 500 °C for 3 h in air.

The α-MnO₂ nanorods were synthesized by a hydrothermal method according to the literature [20]. For preparation of α-MnO₂ nanorods, 1.25 g KMnO₄ and 0.78 g Mn(CH₃COO)₂·4H₂O were mixed in 80 mL deionized water and stirred for 30 min. Then, the mixture was transferred into a Teflon-lined stainless steel autoclave (100 mL) and heated at 160 °C for 12 h. The product was washed and dried at 100 °C overnight. The α-MnO₂/Al₂O₃ catalyst was prepared by mixing the α-MnO₂ sample with γ-Al₂O₃ powder by ball-milling.

2.3. Catalyst characterization

The X-ray diffraction (XRD) patterns of catalysts were recorded on a PANalytical X'Pert PRO X-ray diffractometer (Japan) with Cu Kα radiation (λ = 0.154 nm) at a scan rate of 6 deg (2θ) min⁻¹. X-ray photoelectron spectroscopy (XPS) measurements were performed on a Thermo ESCALAB 250 spectrometer (Vacuum Generators, USA) using Al Kα radiation (1486.6 eV) with constant pass energy of 20 eV. The spectra were corrected by calibrating with the C1s peak at 284.8 eV. Temperature-programmed reduction of H₂ (H₂-TPR) was also performed on a Chemisorption Analyzer (AutoChem 2920). After the samples (100 mg) were pretreated at 400 °C in a flow of 20 vol% O₂/Ar (50 mL/min) for 1 h and cooled

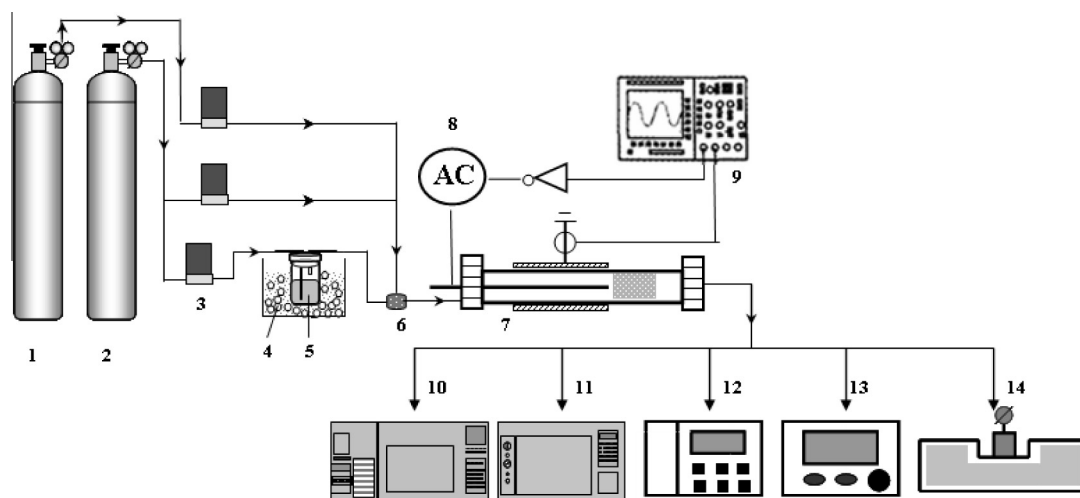


Fig. 1. A schematic diagram of experimental setup. (1) Oxygen, (2) nitrogen, (3) mass flow controller, (4) ice bath, (5) gas bubbler, (6) gas mixer, (7) plasma reactor, (8) AC high voltage supply, (9) oscilloscope, (10) GC-MS, (11) GC, (12) NO_x analyzer, (13) O_3 analyzer, (14) FT-IR.

down to room temperature, the samples were exposed to a flow of 10 vol% H_2/Ar (30 mL/min) at 30 °C for 1 h, followed by raising the temperature to 800 °C at a rate of 10 °C/min. To investigate the Mn content of $\text{Mn}/\text{Al}_2\text{O}_3$, catalysts were dissolved with concentrated HNO_3 and concentrated HCl with a volume ratio of 1:3. Then, the solution was diluted to 50 mL, followed by ICP-OES measurement on an Optima 2000 (Perkin–Elmer Co.). The actual contents of Mn in $\text{Mn}/\text{Al}_2\text{O}_3$ products were close to the nominal contents. Field emission scanning electronic microscopy (FE-SEM) measurements were performed on a SU-8000 electron microscope (Hitachi, Japan).

3. Results and discussion

3.1. Effect of manganese precursor

According to the literature, different precursors used to prepare MnO_x could influence on the dispersion of Mn on supports and activity of catalysts in catalytic oxidation of benzene by ozone [21]. Thus, it is necessary to investigate the effects of precursors used for preparation of $\text{Mn}/\text{Al}_2\text{O}_3$ catalysts on *o*-xylene removal in plasma-catalytic process. Fig. 2 shows *o*-xylene conversion, CO_2 selectivity, and CO_x yield on 6 wt% $\text{Mn}/\text{Al}_2\text{O}_3$ catalysts prepared with different manganese precursors and calcined at 500 °C in the plasma-catalytic system. As shown in Fig. 2, there was only 50% *o*-xylene conversion achieved with air plasma alone at specific energy density (SED) of 18 J/L. The conversion was greatly increased with addition of the $\text{Mn}/\text{Al}_2\text{O}_3$ catalysts. The $\text{Mn}/\text{Al}_2\text{O}_3$ -MA catalyst showed the highest catalytic activity, with 100% conversion of *o*-xylene at a SED as low as 18 J/L. The sequence of catalytic activity was as follows: $\text{Mn}/\text{Al}_2\text{O}_3$ -MA > $\text{Mn}/\text{Al}_2\text{O}_3$ -MS > $\text{Mn}/\text{Al}_2\text{O}_3$ -MN > $\text{Mn}/\text{Al}_2\text{O}_3$ -MC > plasma alone. It is obvious that the *o*-xylene conversion was related to the precursors used for catalyst preparation. The CO_2 selectivity and CO_x yield using $\text{Mn}/\text{Al}_2\text{O}_3$ -MN, $\text{Mn}/\text{Al}_2\text{O}_3$ -MA, and $\text{Mn}/\text{Al}_2\text{O}_3$ -MS catalysts were higher than those achieved using $\text{Mn}/\text{Al}_2\text{O}_3$ -MC or plasma alone.

XRD and XPS experiments were carried out to characterize the structural and valence properties of catalysts. XRD patterns of catalysts prepared with different precursors are shown in Fig. 3. Compared with the typical diffraction peaks of γ - Al_2O_3 , no new peak was observed for $\text{Mn}/\text{Al}_2\text{O}_3$ -MC and $\text{Mn}/\text{Al}_2\text{O}_3$ -MS catalysts. While a new peak appeared at 28.1° for $\text{Mn}/\text{Al}_2\text{O}_3$ -MA, which is one of the diffraction peaks of microcrystalline MnO_2 (PDF#24-0735) [22]. For $\text{Mn}/\text{Al}_2\text{O}_3$ -MN prepared with the manganese nitrate precursor,

sharp diffraction peaks at 28.7°, 32.9°, and 37.3° were observed, which indicated the appearances of MnO_2 and Mn_2O_3 (PDF#24-0735 and PDF#24-0508). The manganese nitrate precursor resulted in the formation of MnO_2 and Mn_2O_3 crystals, and the same result was reported by Rezaei et al. [23].

The XPS analysis was performed to investigate the state and atomic concentration of Mn and oxygen on the surface. Fig. 4 shows the XPS spectra of 6 wt% $\text{Mn}/\text{Al}_2\text{O}_3$. The binding energies at around 643.0 and 641.5 eV could be attributed to the presence of Mn^{4+} and Mn^{3+} species, respectively [22]. It is interesting to note that the Mn^{4+} ratios on the surfaces of $\text{Mn}/\text{Al}_2\text{O}_3$ -MA and $\text{Mn}/\text{Al}_2\text{O}_3$ -MS catalysts were more than 50%, while Mn^{3+} was the dominant species on the surfaces of the $\text{Mn}/\text{Al}_2\text{O}_3$ -MN and $\text{Mn}/\text{Al}_2\text{O}_3$ -MC catalysts, with small amounts of Mn^{4+} (Table 1). The ratio of lattice oxygen (O_α) to surface oxygen or defective oxides (O_β) was the highest for the $\text{Mn}/\text{Al}_2\text{O}_3$ -MA catalyst and the second highest for $\text{Mn}/\text{Al}_2\text{O}_3$ -MS. Thus, structure analysis by XRD and XPS revealed that microcrystalline MnO_2 was helpful for improving the catalytic activity of $\text{Mn}/\text{Al}_2\text{O}_3$ -MA. More Mn^{4+} species and lattice oxygen (O_α) on the surface of the catalyst resulted in the much higher catalytic activity of $\text{Mn}/\text{Al}_2\text{O}_3$ -MA and $\text{Mn}/\text{Al}_2\text{O}_3$ -MS toward total oxidation of *o*-xylene. The reason might be that the effective decomposition of O_3 of MnO_2 (Mn^{4+}) to generate atomic oxide species. Tang et al. have also observed that more Mn^{4+} and the richer lattice oxygen in Mn–Ce composite catalysts were beneficial for the formaldehyde oxidation [24]. Generally, oxidation reactions such as CO and HCHO oxidation on MnO_x catalysts follow the Mars–van Krevelen mechanism [25,26]. The theory study implied that the lattice oxygen concentration could dominate the activity during the reaction [27].

The $\text{Mn}/\text{Al}_2\text{O}_3$ catalysts were subjected to FE-SEM measurements for their morphology. The FE-SEM micrographs displayed that the bulk size of $\text{Mn}/\text{Al}_2\text{O}_3$ -MC was the largest, which might led to the lowest catalytic activity for *o*-xylene conversion in plasma-catalytic system (Fig. 5). Furthermore, the surface areas of $\text{Mn}/\text{Al}_2\text{O}_3$ -MA, $\text{Mn}/\text{Al}_2\text{O}_3$ -MC, $\text{Mn}/\text{Al}_2\text{O}_3$ -MS, and $\text{Mn}/\text{Al}_2\text{O}_3$ -MN were 298.2, 281.4, 284.8, 291.6 m^2/g , respectively. There were only minor differences in surface area among these catalysts, which was not the main effect factor in the different catalytic activity of these catalysts for *o*-xylene conversion.

To examine the redox ability of the catalysts, H_2 -TPR experiments were carried out. Fig. 6 shows the H_2 -TPR profiles of 6 wt% $\text{Mn}/\text{Al}_2\text{O}_3$. Two peaks of H_2 consumption were observed for

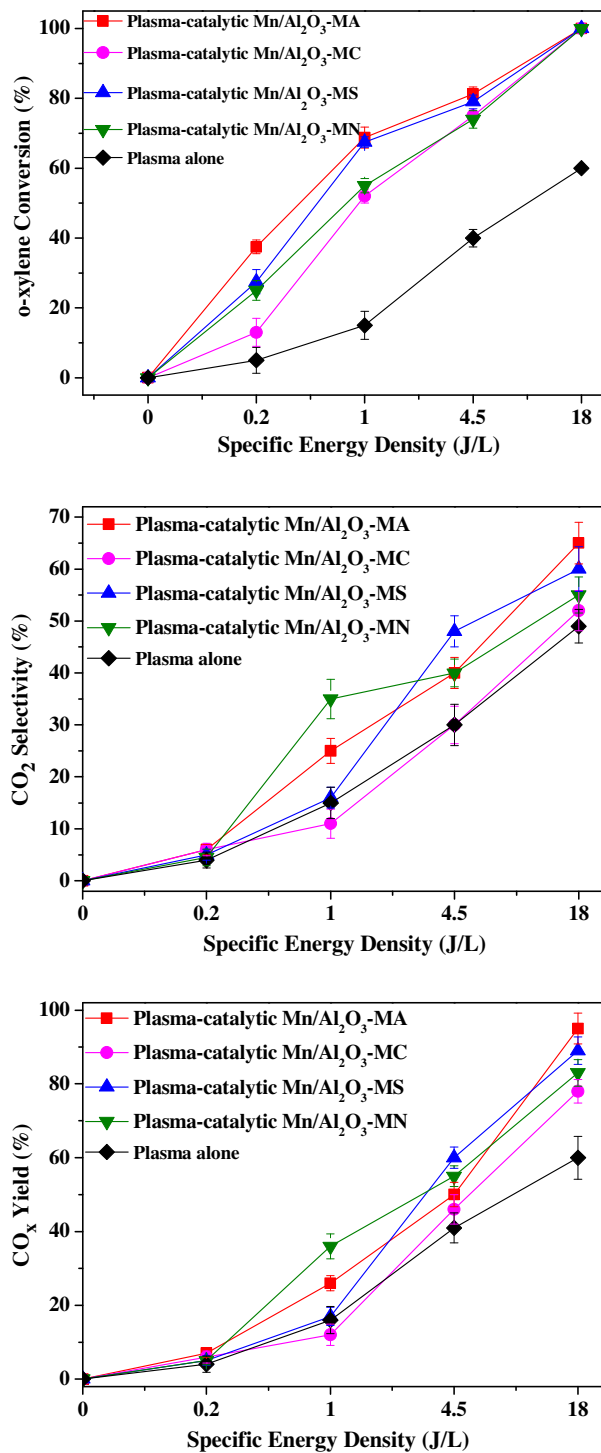


Fig. 2. Effects of manganese precursor for preparation of 6 wt% Mn/Al₂O₃ catalysts on the o-xylene conversion, CO₂ selectivity, and CO_x yield.

Mn/Al₂O₃-MS and Mn/Al₂O₃-MN, and the ratio of the low-temperature peak at 320 °C to the high-temperature peak at 386 °C was about 2. According to the literature, the low-temperature peak should be attributed to reduction of MnO₂ to Mn₃O₄, whereas the high-temperature peak should be attributed to the reduction of Mn₃O₄ to MnO [28]. Only one peak appeared for Mn/Al₂O₃-MA and Mn/Al₂O₃-MC, which suggested that MnO_x (i.e. MnO₂ and Mn₂O₃) should be reduced to MnO directly. The temperature of the reduction peak of Mn/Al₂O₃-MS, Mn/Al₂O₃-

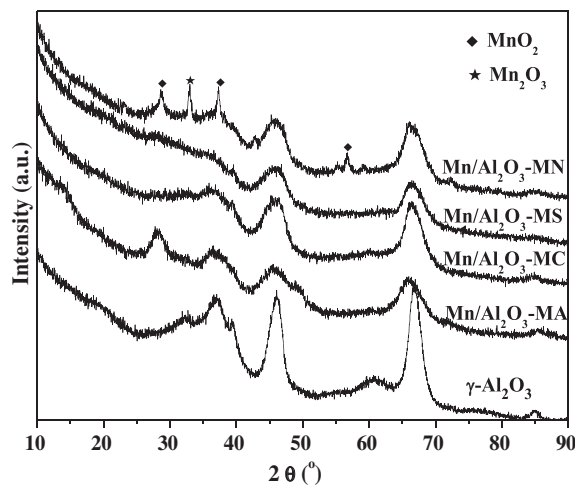


Fig. 3. XRD patterns of 6 wt% Mn/Al₂O₃ catalysts prepared with different precursors.

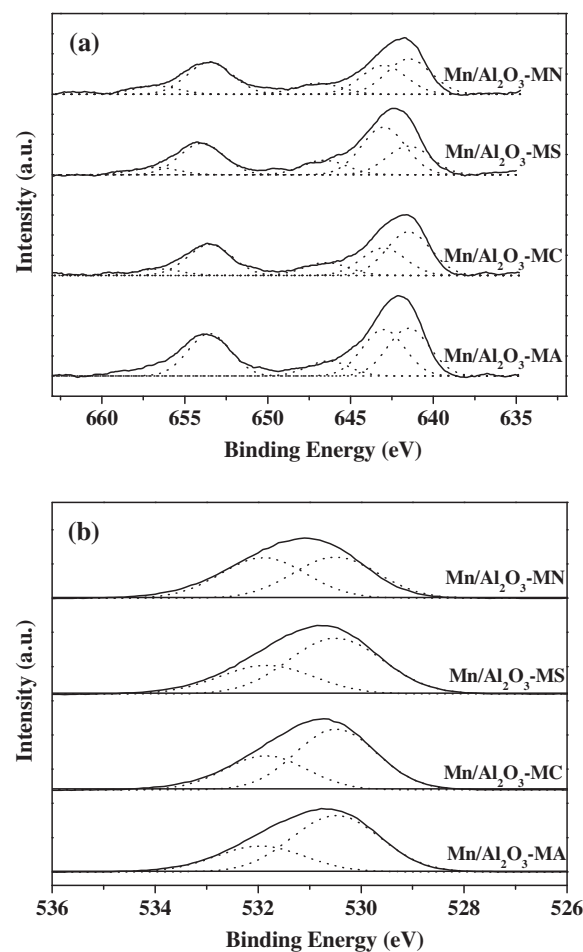


Fig. 4. XPS spectra of 6 wt% Mn/Al₂O₃ catalysts prepared with different precursors (a) Mn 2p XPS spectra, (b) O1s XPS spectra.

MN, and Mn/Al₂O₃-MA was lower than that of Mn/Al₂O₃-MC, which indicated that Mn/Al₂O₃-MS, Mn/Al₂O₃-MN, and Mn/Al₂O₃-MA had high oxidation–reduction ability, which was beneficial for the o-xylene conversion, CO₂ selectivity and CO_x yield.

Table 1
XPS results of the Mn/Al₂O₃ catalysts.

Sample	BE (eV)		Mn ⁴⁺ /(Mn ⁴⁺ + Mn ³⁺) (%)	BE (eV)		O _α /(O _α + O _β) (%)
	Mn ⁴⁺	Mn ³⁺		O _α	O _β	
6 wt% Mn/Al ₂ O ₃						
Mn/Al ₂ O ₃ -MA	643.0	641.5	54	530.5	532.1	75
Mn/Al ₂ O ₃ -MC	643.0	641.5	39	530.5	531.9	64
Mn/Al ₂ O ₃ -MS	643.0	641.5	63	530.5	532.0	71
Mn/Al ₂ O ₃ -MN	643.0	641.5	45	530.5	531.6	50

3.2. Effect of manganese loading amount

The effects of different Mn loading amounts of Mn/Al₂O₃-MA catalysts on the *o*-xylene conversion were investigated. In addition, the actual contents of Mn in all Mn/Al₂O₃ products were close to the prospective contents in the preparation process (Table 2). It was found that *o*-xylene conversion was the highest when 6 wt% Mn/Al₂O₃-MA was used (Fig. 7). XRD patterns showed that 2 and 4 wt% Mn/Al₂O₃-MA had no manganese-related peaks. 6 wt% Mn/Al₂O₃-MA exhibited a prominent MnO₂ microcrystal peak (Fig. 8). Furthermore, 8 wt% Mn/Al₂O₃-MA exhibited a weaker MnO₂ microcrystal peak than 6 wt% Mn/Al₂O₃-MA. XRD results also indicated that weak Mn₃O₄ crystal peaks appeared for 10 wt% Mn/Al₂O₃-MA, and the Mn₃O₄ peak intensity increased with increase of loading amount above 10 wt% Mn (not shown). These results suggested that there was a change of crystal form with increase of manganese loading amount. The analysis of XPS results revealed that 6 wt% Mn/Al₂O₃-MA had the highest Mn⁴⁺ ratio and O_α ratio among Mn/Al₂O₃-MA catalysts with different loading amounts (Table 2). The XRD and XPS results of Mn/Al₂O₃ prepared using different precursors and Mn/Al₂O₃-MA with different loading amounts all proved that the presence of microcrystalline MnO₂, more Mn⁴⁺, and a higher proportion of O_α was beneficial to increase *o*-xylene conversion.

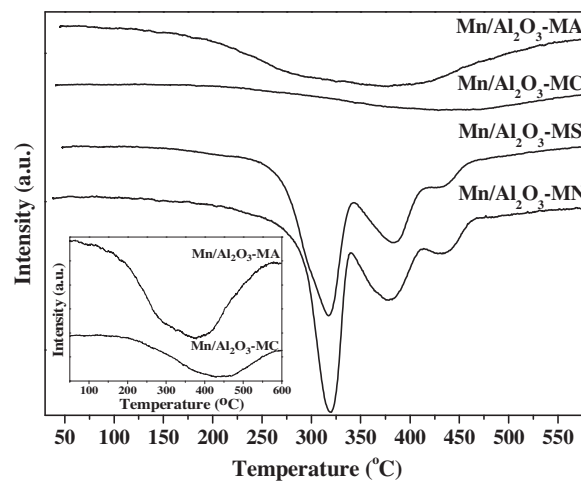


Fig. 6. H₂-TPR profiles of 6 wt% Mn/Al₂O₃ catalysts prepared with different precursors. The inset shows a magnification of the 6 wt% Mn/Al₂O₃-MA and Mn/Al₂O₃-MC profiles.

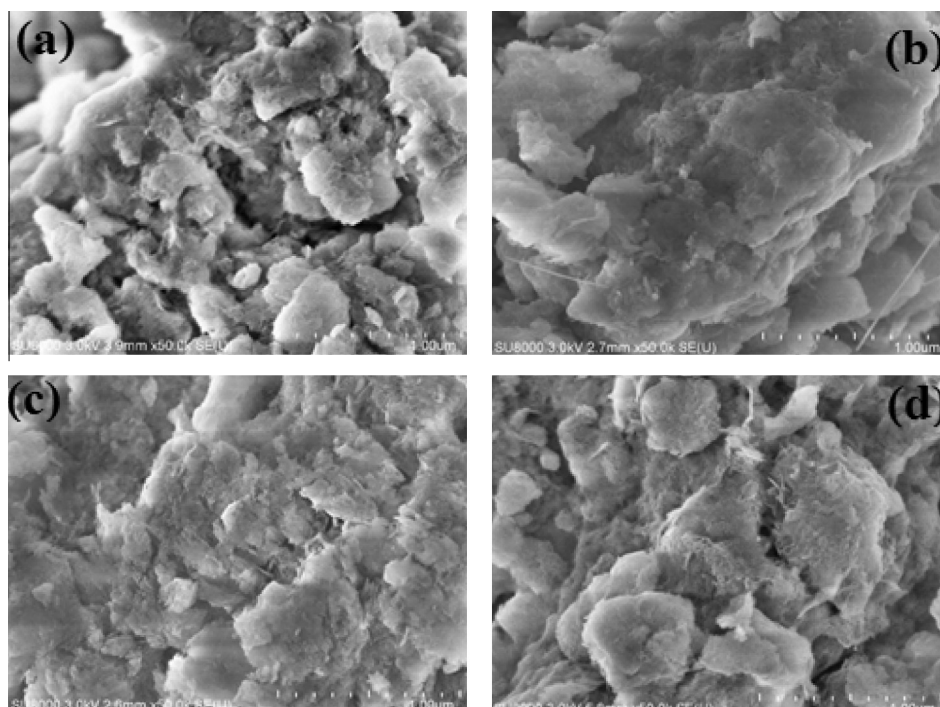


Fig. 5. FE-SEM micrographs of 6 wt% Mn/Al₂O₃ catalysts prepared with different precursors. (a) Mn/Al₂O₃-MA, (b) Mn/Al₂O₃-MC, (c) Mn/Al₂O₃-MS, and (d) Mn/Al₂O₃-MN.

Table 2
XPS and ICP-OES results of the Mn/Al₂O₃ catalysts.

Sample	BE (eV)		Mn ⁴⁺ /(Mn ⁴⁺ + Mn ³⁺) (%)	BE (eV)		O _α /(O _α + O _β) (%)	Mn content detected by ICP-OES (wt%)
	Mn ⁴⁺	Mn ³⁺		O _α	O _β		
Mn/Al ₂ O ₃ -MA							
2 wt%	643.0	641.5	43	530.5	532.0	70	1.9
4 wt%	643.0	641.5	51	530.5	532.0	71	3.8
6 wt%	643.0	641.5	54	530.5	532.1	75	5.9
8 wt%	643.0	641.5	47	530.5	531.9	70	8.2
10 wt%	643.0	641.5	49	530.5	531.9	68	9.7
α-MnO ₂ /Al ₂ O ₃	643.0	641.5	61	530.5	532.0	79	5.8

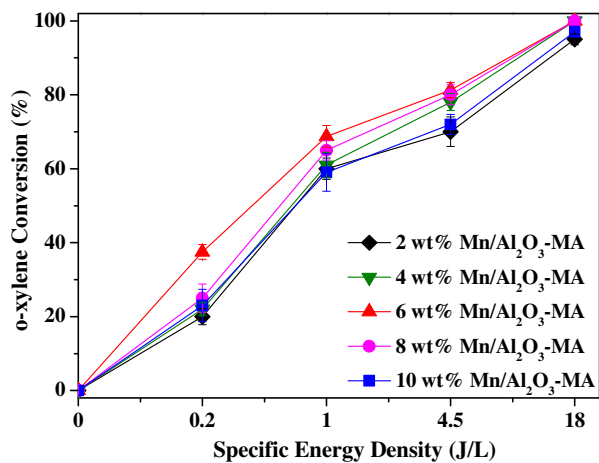


Fig. 7. Effects of loading amounts of Mn/Al₂O₃-MA on the *o*-xylene conversion.

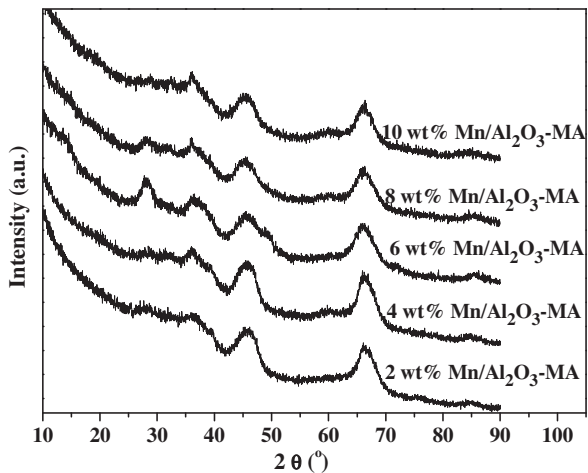
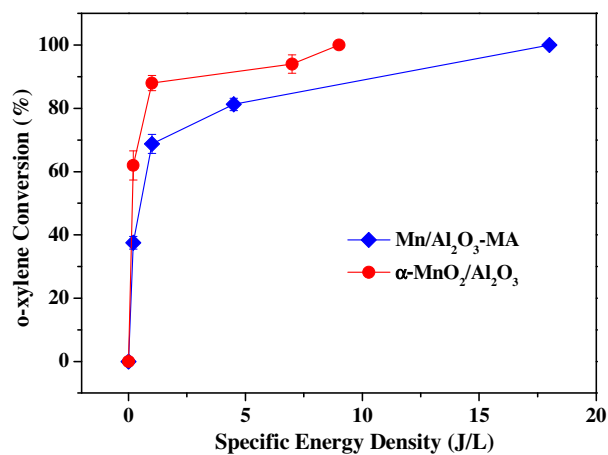


Fig. 8. XRD patterns of Mn/Al₂O₃-MA with different loading amounts.

3.3. Effect of Mn⁴⁺ ratio

According to the above results, it was found that Mn⁴⁺ and O_α on the surface of catalyst were helpful for *o*-xylene oxidation. Therefore, α-MnO₂/Al₂O₃, which had more Mn⁴⁺ and O_α (Table 2), was prepared with a hydrothermal method using manganese acetate as precursor. The catalytic activity of 6 wt% α-MnO₂/Al₂O₃ was compared with that of 6 wt% Mn/Al₂O₃-MA in plasma-catalytic system (Fig. 9). The XRD pattern of α-MnO₂/Al₂O₃ is shown in Fig. 10. Typical α-MnO₂ phases were found [20]. The *o*-xylene conversion efficiency using α-MnO₂/Al₂O₃ was higher than that using Mn/Al₂O₃-MA, and the CO₂ selectivity and CO_x yield slightly increased using α-MnO₂/Al₂O₃ compared with those achieved using Mn/Al₂O₃-MA.

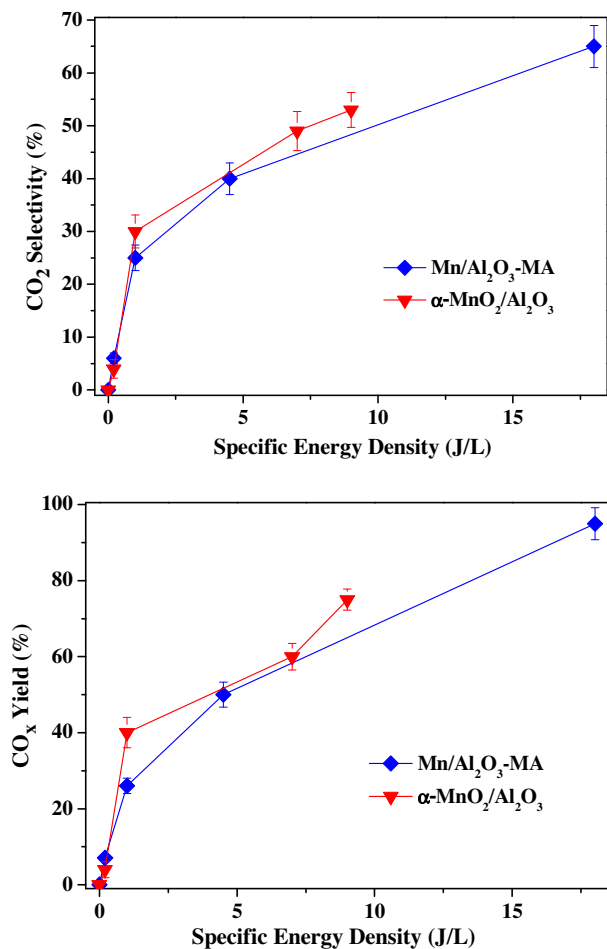


Fig. 9. *o*-xylene conversion, CO₂ selectivity, and CO_x yield using 6 wt% α-MnO₂/Al₂O₃.

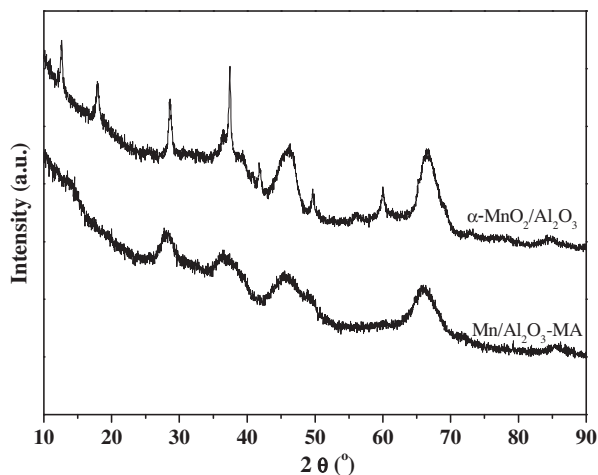


Fig. 10. XRD patterns of 6 wt% α -MnO₂/Al₂O₃.

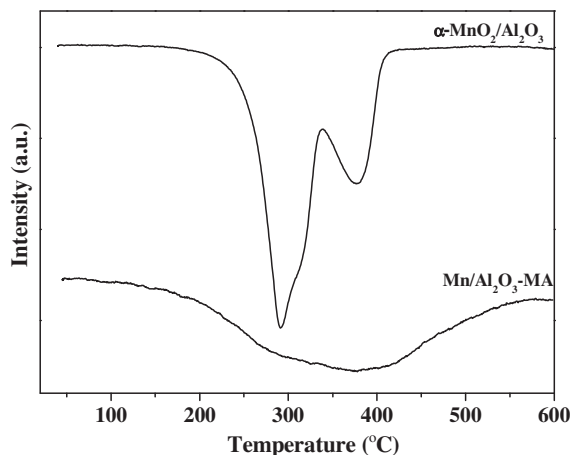


Fig. 11. H₂-TPR profiles of 6 wt% α -MnO₂/Al₂O₃.

Fig. 11 shows the H₂-TPR profiles of 6 wt% α -MnO₂/Al₂O₃ compared with that of 6 wt% Mn/Al₂O₃-MA. The peak intensity of TPR profiles of α -MnO₂/Al₂O₃ at low temperature was much larger than that of Mn/Al₂O₃-MA. These results suggested that oxidation ability of α -MnO₂/Al₂O₃ was higher than that of Mn/Al₂O₃-MA, which was possibly induced by the higher amounts of Mn⁴⁺ and O_α for α -MnO₂/Al₂O₃ and responsible for the increase of *o*-xylene conversion, CO₂ selectivity and CO_x yield when using α -MnO₂/Al₂O₃ catalyst. These results also confirmed the positive role of Mn⁴⁺ and O_α.

3.4. Inhibiting formation of byproducts

To examine the effect of catalysts on suppression of byproduct formation, the outlet O₃ and NO_x concentrations were measured. Fig. 12(a) gives the O₃ outlet concentrations with increase of SED for plasma alone and plasma-catalytic processes. With addition of 6 wt% Mn/Al₂O₃-MA catalyst, the O₃ outlet concentration was greatly decreased. It was clear that most ozone was catalytically decomposed to molecular and highly active atomic oxygen [29]. Those active oxygen species could oxidize *o*-xylene into CO₂. As another byproducts, NO and NO₂ were also monitored in this work. In the case of plasma alone, the NO_x concentration increased to a maximum value of 2.7 ppm with a SED of 18 J/L (Fig. 11(b)). Below 4.5 J/L SED, there was no NO production. Some active molecules and radicals such as O₃, OH and O produced in the discharge

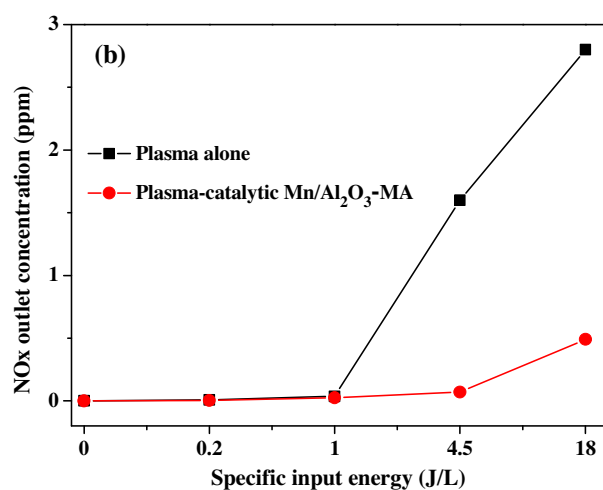
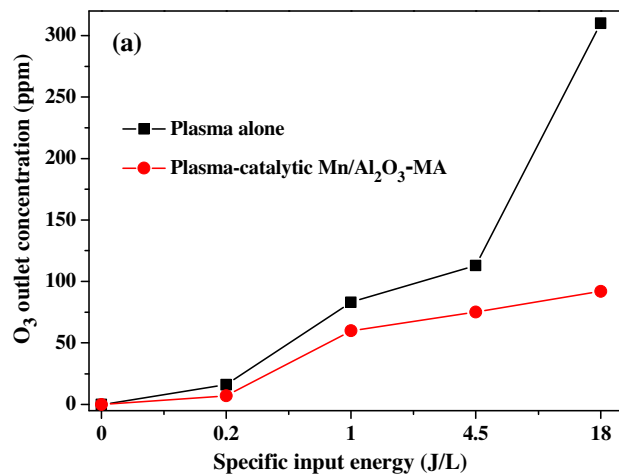


Fig. 12. Byproducts of (a) O₃ and (b) NO_x before and after addition of 6 wt% Mn/Al₂O₃-MA.

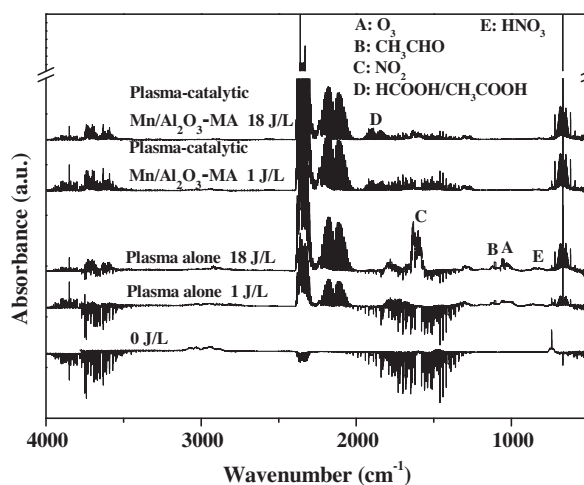


Fig. 13. FT-IR spectra in the processes of plasma and plasma-catalyst (6 wt% Mn/Al₂O₃-MA) oxidation of *o*-xylene.

process could oxidize NO to NO₂, which resulted in less NO production. In contrast, a much lower amount of NO_x was detected with addition of the 6 wt% Mn/Al₂O₃-MA catalyst. Previous research reported that NO_x could be oxidized to HNO₂ and HNO₃ due to oxidation of radicals [30].

Fig. 13 exhibits the main products for plasma and plasma-catalytic processes. Products including CO_2 , CO , NO_2 , O_3 , CH_3CHO , and HNO_3 were observed in the case of plasma alone. The signal intensities of O_3 , NO_2 and CH_3CHO increased with increase of SED, which was consistent with the results obtained by the O_3 and NO_x analyzers. The production of HNO_3 was also observed at about 850 cm^{-1} at higher SED, which should be an oxidation product of NO_x [26]. Products including CO_2 , CO , and $\text{HCOOH}/\text{CH}_3\text{COOH}$, and HNO_3 were observed with addition of 6 wt% $\text{Mn}/\text{Al}_2\text{O}_3$ -MA. The FT-IR waveform for HCOOH is near to that of CH_3COOH , which is difficult to be distinguished. Comparing the major products in the case of plasma alone with the case of catalyst addition, it could be deduced that the $\text{Mn}/\text{Al}_2\text{O}_3$ catalyst could oxidize CH_3CHO to CH_3COOH , and then further oxidize CH_3COOH to CO or CO_2 .

4. Conclusions

In this study, $\text{Mn}/\text{Al}_2\text{O}_3$ catalysts prepared with different precursors were introduced downstream of the discharge zone of DBD plasma system for removal of *o*-xylene. With the introduction of the catalysts, *o*-xylene removal efficiency, CO_2 selectivity and CO_x yield could be significantly improved. The byproducts such as O_3 and NO_x was remarkably reduced by the $\text{Mn}/\text{Al}_2\text{O}_3$ catalysts. The catalysts could oxidize *o*-xylene to CH_3COOH , and then further oxidize CH_3COOH to CO or CO_2 . Among catalysts prepared with four kinds of precursors, the 6 wt% $\text{Mn}/\text{Al}_2\text{O}_3$ catalyst prepared by manganese acetate precursor exhibited the best catalytic activity for *o*-xylene removal, which is due to the presence of micro-crystalline MnO_2 , more Mn^{4+} species, and higher proportion of lattice oxygen on the surface of the catalyst, resulting in high oxidation activity. The *o*-xylene conversion, CO_2 selectivity, and CO_x yield increased with an α - $\text{MnO}_2/\text{Al}_2\text{O}_3$ catalyst that possessed more Mn^{4+} species and lattice oxygen on the surface compared with $\text{Mn}/\text{Al}_2\text{O}_3$ catalysts prepared with the manganese acetate precursor, which also confirmed the positive role of Mn^{4+} species and lattice oxygen.

Acknowledgements

This work was financially supported by the National Natural Science Foundation of China (51208497 and 21422706) and the National High Technology Research and Development Program of China (2012AA062702).

References

- [1] Faisal I. Khan, Alok K. Ghoshal, Removal of volatile organic compounds from polluted air, *J. Loss Prev. Proc.* 13 (2000) 527–545.
- [2] W.B. Li, J.X. Wang, H. Gong, Catalytic combustion of VOCs on non-noble metal catalysts, *Catal. Today* 148 (2009) 81–87.
- [3] H.M. Lee, M.B. Chang, Abatement of gas-phase *p*-xylene via dielectric barrier discharges, *Plasma Chem. Plasma P.* 23 (2003) 541–558.
- [4] V. Demidyuk, J. Christopher Whitehead, Influence of temperature on gas-phase toluene decomposition in plasma-catalytic system, *Plasma Chem. Plasma P.* 27 (2007) 85–94.
- [5] Y.Z. Li, Z.Y. Fan, J.W. Shi, Z.Y. Liu, W.F. Shangguan, Post plasma-catalysis for VOCs degradation over different phase structure MnO_2 catalysts, *Chem. Eng. J.* 241 (2014) 251–258.
- [6] W.Z. Wang, H.L. Wang, T.L. Zhu, X. Fan, Removal of gas phase low-concentration toluene over Mn, Ag and Ce modified HZSM-5 catalysts by periodical operation of adsorption and non-thermal plasma regeneration, *J. Hazard. Mater.* 292 (2015) 70–78.
- [7] M.J. Lu, R. Huang, J.L. Wu, M.L. Fu, L.M. Chen, D.Q. Ye, On the performance and mechanisms of toluene removal by $\text{FeO}_x/\text{SBA-15}$ -assisted non-thermal plasma at atmospheric pressure and room temperature, *Catal. Today* 242 (2015) 259–265.
- [8] Y.F. Guo, D.Q. Ye, K.F. Chen, J.C. He, W.L. Chen, Toluene decomposition using a wire-plate dielectric barrier discharge reactor with manganese oxide catalyst in situ, *J. Mol. Catal. A Chem.* 245 (2006) 93–100.
- [9] T.L. Zhu, M.Y. Wang, X.M. Li, Removal of low-concentration BTX in air using a combined plasma catalysis system, *Chemosphere* 75 (2009) 1301–1306.
- [10] Ch. Subrahmanyam, A. Renken, L. Kiwi-Minsker, Catalytic non-thermal plasma reactor for abatement of toluene, *Chem. Eng. J.* 160 (2010) 677–682.
- [11] A. Ogata, K. Yamanouchi, K. Mizuno, S. Kushiya, T. Yamamoto, Decomposition of benzene using alumina-hybrid plasma reactors, *IEEE T. Ind. Appl.* 35 (1999) 1289–1295.
- [12] A. Ogata, H. Einaga, H. Kabashima, S. Futamura, S. Kushiya, H.H. Kim, Effective combination of nonthermal plasma and catalysts for decomposition of benzene in air, *Appl. Catal. B Environ.* 46 (2003) 87–95.
- [13] H.H. Kim, S.M. Oh, A. Ogata, S. Futamura, Decomposition of gas-phase benzene using plasma-driven catalyst (PDC) reactor packed with Ag/TiO_2 catalyst, *Appl. Catal. B Environ.* 56 (2005) 213–220.
- [14] J. Li, S.T. Han, S.P. Bai, X.C. Shi, S.L. Han, H. Song, Y.K. Pu, X.M. Zhu, W.C. Chen, Effect of $\text{Pt}/\gamma\text{-Al}_2\text{O}_3$ catalyst on nonthermal plasma decomposition of benzene and byproducts, *Environ. Eng. Sci.* 28 (2011) 395–403.
- [15] U. Roland, F. Holzer, F.D. Kopinke, Combination of non-thermal plasma and heterogeneous catalysis for oxidation of volatile organic compounds. Part 2. Ozone decomposition and deactivation of $\gamma\text{-Al}_2\text{O}_3$, *Appl. Catal. B Environ.* 58 (2005) 217–226.
- [16] Alice M. Harling, David J. Glover, J. Christopher Whitehead, K. Zhang, The role of ozone in the plasma-catalytic destruction of environmental pollutants, *Appl. Catal. B Environ.* 90 (2009) 157–161.
- [17] B. Dhandapani, S.T. Oyama, Gas phase ozone decomposition catalysts, *Appl. Catal. B Environ.* 11 (1997) 129–166.
- [18] H. Einaga, N. Maeda, Y. Teraoka, Effect of catalyst composition and preparation conditions on catalytic properties of unsupported manganese oxides for benzene oxidation with ozone, *Appl. Catal. B Environ.* 142–143 (2013) 406–413.
- [19] L.L. Ye, F.D. Feng, J. Liu, Z. Liu, K.P. Yan, Plasma induced toluene decomposition on alumina-supported Mn-based composite oxides catalysts, *J. Phys. Conf. Ser.* 418 (2013) 012116.
- [20] S.H. Liang, F. Teng, G. Bulgan, R.L. Zong, Y.F. Zhu, Effect of phase structure of MnO_2 nanorod catalyst on the activity for CO oxidation, *J. Phys. Chem. C* 112 (2008) 5307–5313.
- [21] J.H. Park, J.M. Kim, M. Jin, J.K. Jeon, S.S. Kim, S.H. Park, S.C. Kim, Y.K. Park, *Nanoscale Res. Lett.* 7 (2012) 2–5.
- [22] Y.S. Wu, Y. Lu, C.J. Song, Z.C. Ma, S.T. Xing, Y.Z. Gao, A novel redox-precipitation method for the preparation of $\alpha\text{-MnO}_2$ with a high surface Mn^{4+} concentration and its activity toward complete catalytic oxidation of *o*-xylene, *Catal. Today* 201 (2013) 32–39.
- [23] E. Rezaei, J. Soltan, Low temperature oxidation of toluene by ozone over $\text{MnO}_x/\gamma\text{-alumina}$ and $\text{MnO}_x/\text{MCM-41}$ catalysts, *Chem. Eng. J.* 198–199 (2012) 482–490.
- [24] X.F. Tang, Y.G. Li, X.M. Huang, Y.D. Xu, H.Q. Zhu, J.G. Wang, W.J. Shen, $\text{MnO}_x\text{-CeO}_2$ mixed oxide catalysts for complete oxidation of formaldehyde: effect of preparation method and calcination temperature, *Appl. Catal. B Environ.* 62 (2006) 265–273.
- [25] R. Xu, X. Wang, D.S. Wang, K.B. Zhou, Y.D. Li, Surface structure effects in nanocrystal MnO_2 and Ag/MnO_2 catalytic oxidation of CO, *J. Catal.* 237 (2006) 426–430.
- [26] J.H. Zhang, Y.B. Li, L. Wang, C.B. Zhang, H. He, Catalytic oxidation of formaldehyde over manganese oxides with different crystal structures, *Catal. Sci. Technol.* 5 (2015) 2305–2313.
- [27] W.Y. Song, E.M. Hensen, A computational DFT study of CO oxidation on a Au nanorod supported on CeO_2 (110): on the role of the support termination, *Catal. Sci. Technol.* 3 (2013) 3020–3029.
- [28] F. Kapteijn, L. Smgoredjo, A. Andreml, J.A. Mouhjn, Activity and selectivity of pure manganese oxides in the selective catalytic reduction of nitric oxide with ammonia, *Appl. Catal. B Environ.* 3 (1994) 173–189.
- [29] S. Futamura, A. Zhang, H. Einaga, H. Kabashima, Involvement of catalyst materials in nonthermal plasma chemical processing of hazardous air pollutants, *Catal. Today* 72 (2002) 259–265.
- [30] A. Ogata, K. Miyamae, K. Mizuno, S. Kushiya, M. Tezuka, Decomposition of benzene in air in a plasma reactor: effect of reactor type and operating conditions, *Plasma Chem. Plasma P.* 22 (2002) 537–552.